Journal of Materials Chemistry A

PAPER

View Article Online
View Journal | View Issue

Cite this: J. Mater. Chem. A, 2017, 5, 10021

Received 4th April 2017
Accepted 2nd May 2017

DOI: 10.1039/c7ta02913f

rsc.li/materials-a

$Na_{0.35}MnO_2$ as an ionic conductor with randomly distributed nano-sized layers†

Arturas Adomkevicius,[ab] Laura Cabo-Fernandez,[a] Tzu-Ho Wu,[ab] Tzu-Man Ou,[b] Ming-Guan Chen,[b] Yuri Andreev,*[c] Chi-Chang Hu*[b] and Laurence J. Hardwick *[a]

Here we show that through a straightforward synthesis it is possible to create a bulk material, $Na_{0.35}MnO_2$, with isolated sheets. Due to such an arrangement of the oxide layers, this ionic conductor was found to be genuinely pseudocapacitive, with charge storage not limited by diffusion of ions between stacked layers, resulting in capacitance values of 190 F g^{-1} under exceptionally high current rates of up to 200 A g^{-1}.

Introduction

Manganese oxides have been widely investigated for supercapacitor applications.[1–4] Numerous different compounds based around MnO_x, as well as variations in structure and morphology have been reported.[5–10] One of the more promising materials is cation pre-intercalated manganese oxides. Here the cation located in-between the MnO_2 layers is involved in the charge storage mechanism; thus enabling the electrolyte to maintain both a stable salt concentration and ionic conductivity during charge and discharge.[11] Limitations to intercalation-based charge storage from solid state diffusion result in the high diffusion barrier of cations. This reduces the power performance, although pseudocapacitance may be increased at very low currents or scan rates.[12–15] However, important influences of dimension and crystalline size of cation-pre-intercalated MnO_2 nanosheets on the cation diffusion rate within 2D MnO_2 have not yet been fully explored.

Materials of reduced dimensionality have been under intense investigation since the discovery of Buckminsterfullerene (0D),[16] carbon nanotubes (1D)[17] and graphene (2D).[18] In particular, 2D materials are being critically examined for a whole host of applications in energy, materials, and engineering.[19–23] The challenge of fully utilising 2D materials is the ability to scale up the synthesis in concert with maintaining the remarkable material properties reported from studies of single isolated flakes.[24–26]

Isolated in suspension, 2D sheets, once sedimented, tend to stack, forming a 3D-ordered material with either ideal crystallographic interlayer registry or restricted to equidistant layers.[23,27–31] This inevitably leads to the loss of the unique 2D properties, such as vastly accessible surface area. The challenge of making truly 2D materials is always accompanied by the difficulty of establishing their structure using direct, powder diffraction, methods since the commonly used diffraction methodologies are not adequately suited for materials with lower than perfectly 3D ordering. Powder diffraction data from the literature, when provided, indicate that the majority of reportedly 2D-material powders routinely have the diffraction pattern similar to their 3D counterparts albeit often with a small and anisotropic crystallite size.[32,33] Here we show that a reliable structural model of a 2D-ordered compound, in this case $Na_{0.35}MnO_2$, can be obtained through powder diffraction data and the fundamental equation of Debye. As a consequence, through the interactive influences of both dimension and crystalline size of the cation-pre-intercalated MnO_2 nanosheets, the capacitance was found not to be limited by solid-state diffusion.

Experimental

Material preparation

The synthesis route for sodium pre-intercalated manganese oxide (Na_xMnO_2) was devised where conditions would promote the formation of a disordered material. 3 mM $MnSO_4$ (aq.) (Hayashi Pure Chemical, Japan) and 2 mM $KMnO_4$ (aq.) (Shimakyu's Pure Chemical, Japan) were added together at 30 °C, followed by the addition of 15 mM Na_2SO_4 (Showa Chemical Co. Ltd, Japan). After mixing, the pH of the solution was adjusted to 12.3 *via* dropwise addition of 1 M NaOH (aq.) and was then transferred to a Teflon-lined pressure vessel and heated within an oven (Memmert) to 75 °C (±0.5 °C) for 12 h. After cooling, the precipitate was filtered and washed with deionised water. The mild temperatures and the inclusion of a molar excess of alkali

[a]Stephenson Institute for Renewable Energy, Department of Chemistry, University of Liverpool, Chadwick Building, Peach Street, Liverpool, L69 7ZF, UK. E-mail: hardwick@liverpool.ac.uk

[b]Department of Chemical Engineering, National Tsing Hua University, Hsin-Chu, 30013 Taiwan. E-mail: cchu@che.nthu.edu.tw

[c]School of Chemistry, University of St Andrews, St Andrews, Scotland, KY16 9ST, UK. E-mail: ya@st-andrews.ac.uk

† Electronic supplementary information (ESI) available: ICP-OES, PXRD, TEM, electrochemical characterisation, X-ray absorption spectroscopy and BET. See DOI: 10.1039/c7ta02913f

metal cations with respect to manganese disrupt the formation of a highly crystalline material. By carrying out the synthesis under strict temperature control, we were able to obtain a single phase product. The stoichiometry of resultant material was determined as $Na_{0.35}MnO_2$ by elemental analysis *via* inductively coupled plasma optical emission spectrometry, ICP-OES (see ESI†).

Electrode preparation

The coating slurry was prepared by mixing 70 wt% of $Na_{0.35}MnO_2$, 20 wt% of carbon black (Vulcan XC72, USA), and 10 wt% of poly(vinylidene difluoride) (PVdF) binder (Sigma-Aldrich), which was dispersed in *N*-methyl-2-pyrrolidone (NMP, Tedia Company Inc. USA) followed by sonication for 60 min. The slurry was coated on a graphite substrate (1 cm × 1 cm) and dried in an oven for 12 h at 45 °C to obtain the electrodes. The mass of $Na_{0.35}MnO_2$ as the electroactive material in this study was fixed to be 0.5 mg cm^{-2}, resulting in the total mass loading of 0.71 mg cm^{-2}.

Structural characterisation

X-ray powder diffraction data were collected in a capillary mode on PANalytical Empyrean using Mo $K\alpha_{1,2}$ radiation (see ESI† for more details). Raman spectra were recorded within an argon containing airtight cell using a Raman microscope (Renishaw in Via), with the He–Ne laser (632.8 nm) illumination focused through an inverted microscope (Leica), *via* a 50× objective lens (Leica). In order to avoid local heating by the laser, the sample surface exposure was carefully controlled *via* the use of an appropriate filter. The acquisition time for each spectrum was 300 s. Scanning electron microscopic (SEM) images were collected with a field-emission scanning electron microscope (FE-SEM, Hitachi SU8010). Transmission electron microscopic (TEM) and selected-area electron diffraction (SAED) images were recorded using a JEOL, JEM 3010 microscope with an accelerating voltage of 300 kV and a high-resolution transmission electron microscope (HRTEM, JEOL, 2100F) at 200 kV. Nitrogen adsorption and desorption isotherms were measured at 77.3 K by means of the Micromeritics ASAP 2020 surface area and porosity analyser.

Electrochemical characterisation

Cyclic voltammetry (CV) and galvanostatic charge–discharge (GCD) tests of as-prepared samples were conducted on an electrochemical station (CHI 1128C, CH Instruments, USA). The specific capacitance of $Na_{0.35}MnO_2$ was calculated from the discharge curves:

$$C_{S,Mn} = \frac{I \times \Delta t}{m \times \Delta V} \quad (1)$$

where $C_{S,Mn}$, m, ΔV, I, and Δt are the specific capacitance of $Na_{0.35}MnO_2$, mass loading of $Na_{0.35}MnO_2$ on the substrate, potential window of discharge tests, applied current, and discharge time, respectively.[34]

Results and discussion

Powder X-ray diffraction pattern of $Na_{0.35}MnO_2$, shown in Fig. 1 and ESI,† is characterised by a very low signal-to-noise ratio, indicating that the compound is largely disordered. The regions of the pattern representing coherent scattering are reminiscent of those previously calculated for a single layer of MnO_2 and contain broad asymmetric peaks.[35]

The structure of the ordered regions has been determined using a newly developed refinement method based on the fundamental scattering equation of Debye[36] and thus far employed to determine the shape and size of 3D nanoparticles[37] and of 2D graphene layers in partially disordered carbon blacks.[38] A single infinite layer of the manganese oxide from the structure of hexagonal H-birnessite[39] was used as a starting model for the refinement. The shape of each trial layer was assumed to be an elliptical cylinder, with the axes' lengths of the ellipse, lattice parameters, amplitudes of mean-square displacements of atoms and the directional angle of the cylindrical cut-out serving as variables in the refinement.

The entire experimental powder diffraction profile of $Na_{0.35}MnO_2$ fits exceptionally well ($\chi^2 = 1.6$), see Fig. 1, by the pattern calculated from the fragment of a MnO_2 layer shown in Fig. 2(a), with Mn–O distances of 0.1863 nm and the lengths of the elliptical axes of 2 and 4 nm. A nano-sized region of an individual layer fitting the whole experimental data proves that such region represents all the order within the powder. There is no crystallographic registry, or even stacking in any regular fashion, of the MnO_2 layers, in Fig. 2(b), and no ordered pattern in the positions of the sodium atoms.

The structure and domain size of $Na_{0.35}MnO_2$ were observed by field emission scanning electron microscopy (FE-SEM) and transmission electron microscopy (TEM), see Fig. 3. The powder consists of particles 200–250 nm in length and 150–200 nm in width, from Fig. 3(a) and (b). Moreover, the high-magnification SEM image in Fig. 3(b) shows the aggregates of $Na_{0.35}MnO_2$ primary particles without a clear inter-particle boundary.

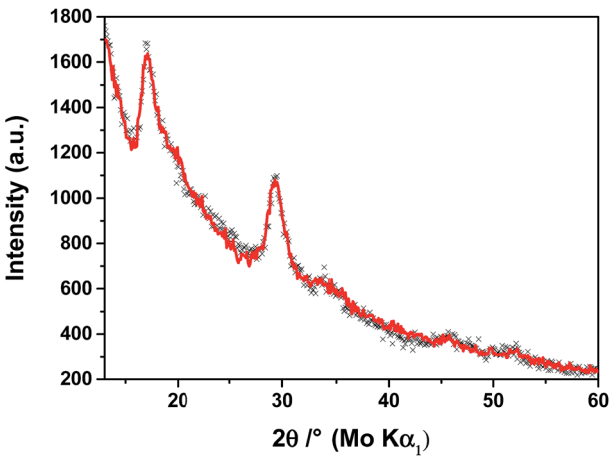

Fig. 1 Experimental (black crosses) and calculated, using the best-fit model obtained from the Debye refinement, (red line) X-ray powder diffraction patterns of $Na_{0.35}MnO_2$.

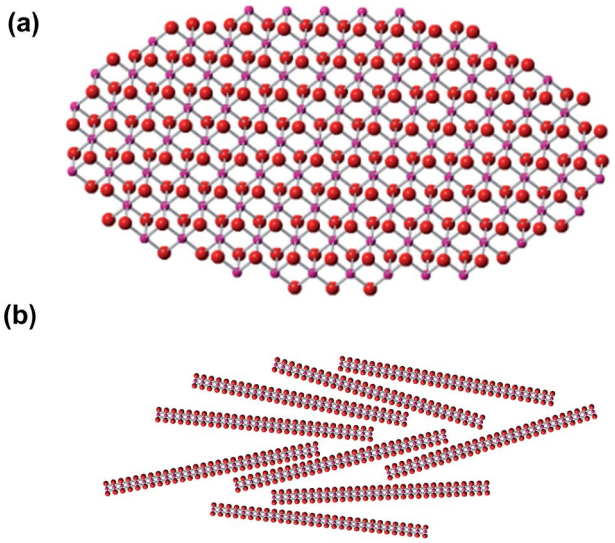

Fig. 2 Structural model. (a) Top view of the ordered region within a single MnO_2 layer, from which the powder diffraction pattern in Fig. 1 was calculated. Magenta – manganese; red – oxygen, (b) schematic profile view of a possible arrangement of the ordered regions within layers of $Na_{0.35}MnO_2$.

TEM images in Fig. 3(c)–(e) show that domains consist of poorly ordered and randomly stacked MnO_2 layers. The disperse rings in the selected area electron diffraction (SAED) pattern indicate the poor crystallinity of $Na_{0.35}MnO_2$ as shown in Fig. 3(f). It is important to highlight that $Na_{0.35}MnO_2$ is sensitive to the high energy electron beam and if viewed at higher magnifications (>×800k), it transforms to the hausmannite crystalline phase of Mn_3O_4 (see ESI†). The lattice parameters are typical of Mn_3O_4, and the change in crystallinity is confirmed by defined rings within the SAED image and Raman spectroscopy.[40,41] The sheet length of the ordered Mn_3O_4 layers formed under the electron beam are seen to be either in the 2 nm or 4–5 nm range. This indirect observation corroborates our structure model.

The Raman spectrum of $Na_{0.35}MnO_2$ (Fig. 4) resembles some of the characteristics of the spectrum typically reported for Na-birnessite MnO_2 and all four fitted peaks can be assigned to Mn–O vibrational modes (Table 1).[41] In particular, the Raman bands at 651 cm^{-1}, 577 cm^{-1} and 502 cm^{-1} can be assigned respectively to the symmetric stretching vibration of Mn–O band of MnO_6 groups, Mn–O stretching within the basal plane of the MnO_6 sheet and Mn–O stretching vibration of MnO_6 octahedra.[42,43]

The lack of order in the positions of the sodium atoms is supported by the absence of bands associated with the stretching modes of NaO_6 octahedron and NaO_4 tetrahedron for Na-birnessite that are typically observed below 450 cm^{-1}.[43,44]

The current response was found to be linearly proportional to the scan rate of CV when the scan rate is varied between 5 and 1000 mV s^{-1} (Fig. 5(a)), thereby illustrating that $Na_{0.35}MnO_2$ is genuinely pseudocapacitive, where the charge storage mechanism is based on the surface redox processes (see ESI†).

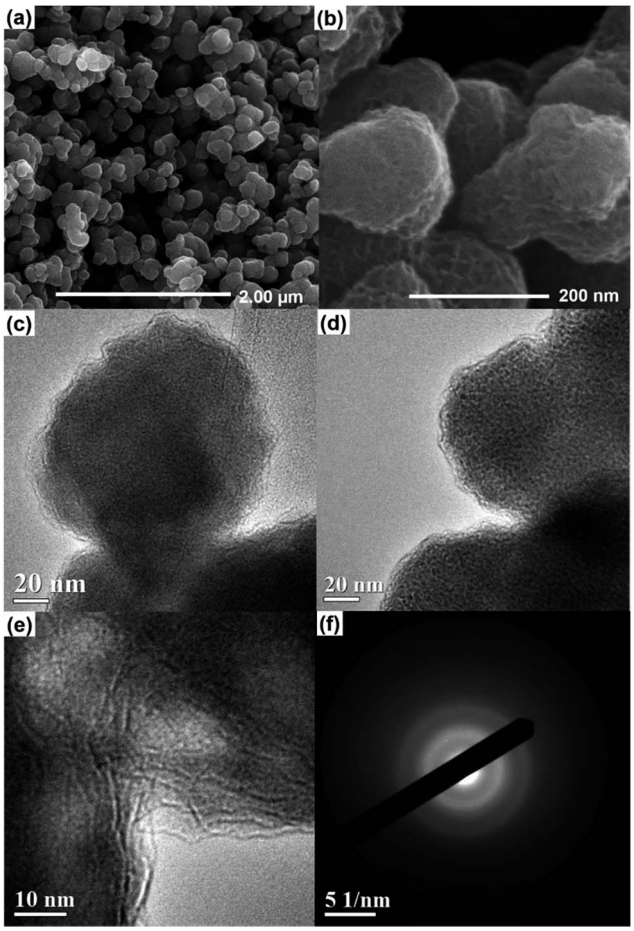

Fig. 3 FE-SEM images of $Na_{0.35}MnO_2$ at low (a) and high (b) magnifications. (c–e), TEM images of $Na_{0.35}MnO_2$ and (f), a selected area electron diffraction (SAED) pattern.

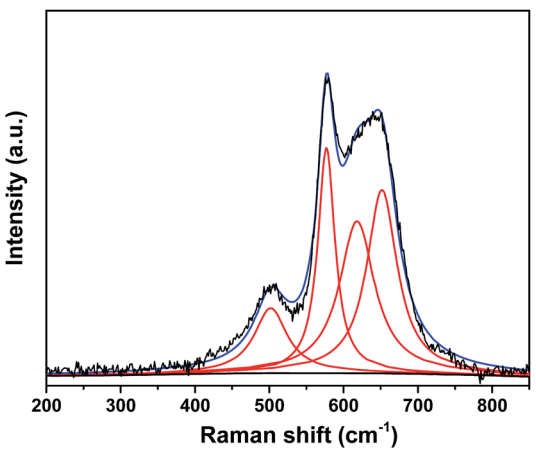

Fig. 4 Lorentz fitting of Raman spectrum of $Na_{0.35}MnO_2$ (blue line is the envelope of total of the fitted peaks).

The ideal capacitive performance is demonstrated by the near-rectangular CV curve measured at 100 mV s^{-1} (Fig. 5(b)), which is in contrast to chemically similar compounds that display distinct redox peaks in their CVs.[15,47] Moreover,

Table 1 Fitted Raman band positions and full width at half-maximum (FWHM) of $Na_{0.35}MnO_2$. Bands are assigned according to the literature[43,45,46]

Position (cm^{-1})	FWHM (cm^{-1})	Band	Vibrational modes
651	49	υ_1	Symmetric stretching vibration of Mn–O band in the MnO_6 octahedra
618	57	υ_2	Mn–O lattice vibration
577	27	υ_3	Mn–O lattice vibration of the basal plane of the MnO_2 sheets
502	53	υ_4	Mn–O stretching vibration of MnO_6 octahedra

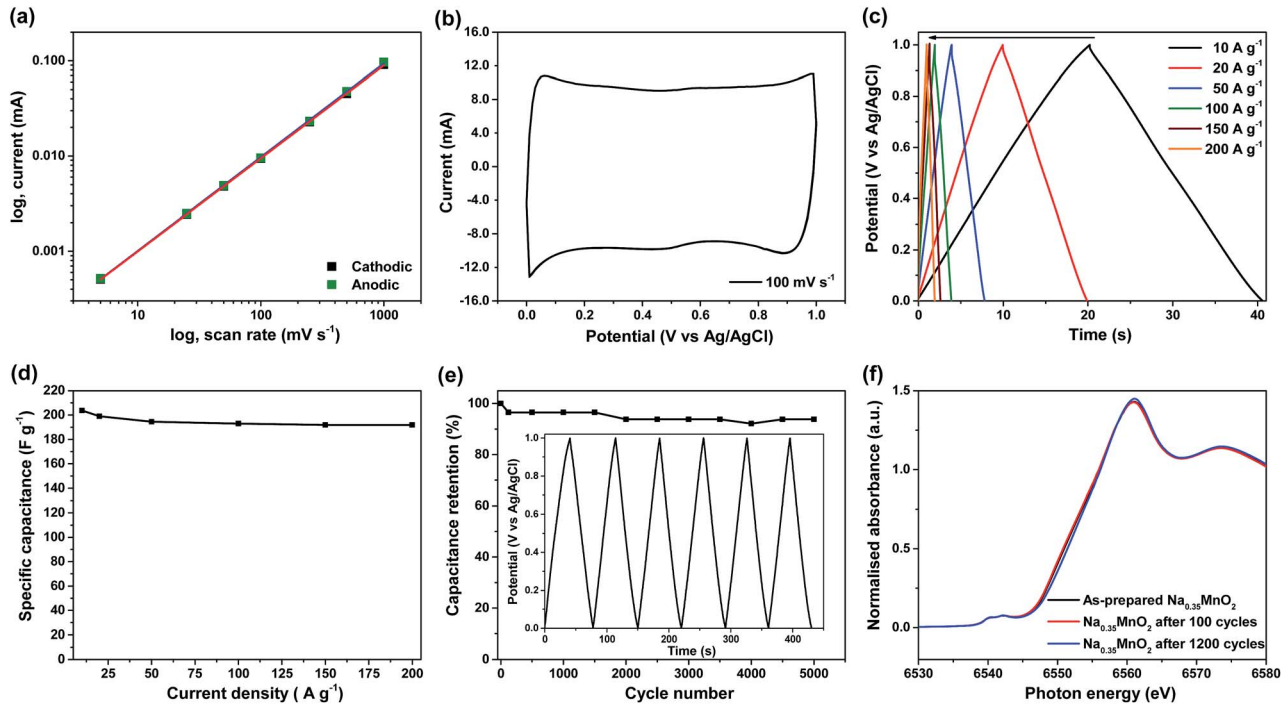

Fig. 5 (a) Plots of cathodic and anodic currents of the $Na_{0.35}MnO_2$ electrode *versus* scan rates between 5 and 1000 mV s^{-1} in 0.5 M Na_2SO_4. (b) A cyclic voltammogram of $Na_{0.35}MnO_2$ measured at 100 mV s^{-1}, (c) the galvanostatic charge–discharge curves at 10–200 A g^{-1}, (d) specific capacitance of $Na_{0.35}MnO_2$ against the charge–discharge current density at 10–200 A g^{-1}, (e) the capacitance retention as function of the cycle number; where the inset shows charge/discharge curves of the $Na_{0.35}MnO_2$ between 0 and 1 V (*vs.* Ag/AgCl) at a current density of 5 A g^{-1} in 0.5 M Na_2SO_4 and 2 mM $NaHCO_3$ and (f) X-ray absorption near-edge structure (XANES) spectra of as-prepared $Na_{0.35}MnO_2$ (black), and after 100 cycles (red) and 1200 cycles (blue) of charge–discharge.

rectangular CV curves were measured from scan rates between 5 to 1000 mV s^{-1} (see ESI†). The pseudocapacitive nature of $Na_{0.35}MnO_2$ can be further supported by a low specific surface area of 15 m^2 g^{-1}, using the Brunauer–Emmett–Teller (BET) method (see ESI†), with a total porosity of 0.0595 cm^3 g^{-1}. For bulk MnO_2, pseudocapacitance is derived from the redox activity of manganese at the surface/near surface region of the active material[1] whereas the interior of MnO_2 crystals remains mostly inactive.[48] Typically, the charge storage mechanism in neutral pH electrolytes is based on the extraction of superficially adsorbed/absorbed Na^+ cations according to the reaction:

$$(MnO_2)_{surface} + Na^+ + e^- \leftrightarrow (MnO_2{}^-Na^+)_{surface} \quad (2)$$

Once within the aqueous electrolyte, we surmise that Na^+ and H_2O are located randomly between the MnO_2 sheets, permitting redox processes for both the surface and interior of the sheets. The arrangement of the sheets allow facile exchange of Na^+ and H_2O from and to the bulk electrolyte during charge and discharge. Na^+ has a dual role of allowing the formation of a disordered material during synthesis and being ready present to partake in the initial exchange of speciation at the interface during electrode polarisation.

To further explore the advanced pseudocapacitive characteristics of the $Na_{0.35}MnO_2$, galvanostatic charge–discharge measurements were carried out at various current densities and the results are shown in Fig. 5(c). The charge curves measured at all current densities are highly symmetrical to their corresponding discharge counterparts, revealing the ideal capacitive property of the $Na_{0.35}MnO_2$ electrode. The specific capacitance, ($C_{S,Mn}$) of $Na_{0.35}MnO_2$ obtained at 10 A g^{-1}, calculated from the discharge curves in Fig. 5(c) was 204 F g^{-1} (see Experimental). The *iR* drop (0.07 V) is low, even at the high current density of 100 A g^{-1}, indicating low internal resistance of the electrode

material. Accordingly, the $C_{S,Mn}$ values of $Na_{0.35}MnO_2$ measured at 20, 50, 100, 150, and 200 A g^{-1} are equal to 199, 195, 193, 192 and 192 F g^{-1}, respectively (see Fig. 5(d)). 94% capacitance is retained even when the current density has been increased by a factor of 20. Fig. 5(e) shows the cycle-life data of the $Na_{0.35}MnO_2$ in which no significant capacitance loss (<5%) was observed after 5000 charge–discharge cycles.

The stability of $Na_{0.35}MnO_2$ is supported by the synchrotron X-ray absorption measurements whereby the X-ray absorption near-edge structure (XANES) spectra demonstrate similar features for as-prepared and cycled (100 and 1200 cycles) $Na_{0.35}MnO_2$. A multiple structure of pre-edge region at *ca.* 6541 eV can be observed for $Na_{0.35}MnO_2$ (Fig. 5(f) and ESI†), which are attributed to the partially allowed transition of a 1s electron to an unoccupied 3d orbital.[49] The split in the pre-edge peaks was reported as the separation of degenerated 3d levels under the octahedral crystal field, which are corresponding to 1s to 3d (t_{2g}) and 1s to 3d (e_g) transitions, respectively.[49] The main absorption edge around 6560 eV is assigned to the purely dipole-allowed 1s to 4p transition.[49] According to the quasi-linear relationship, the Mn oxidation state of the as-prepared sample is 3.57, indicating a minor sub-stoichiometric presence of oxygen within the material (*i.e.* $Na_{0.35}MnO_{1.96}$). For the cycled samples, the Mn oxidation state and XANES features remain similar, indicating the cycle stability of $Na_{0.35}MnO_2$, where the oxidation state decreases marginally from 3.57 to 3.45 over 1200 cycles (see ESI†).

The outstanding capacitive performance at high currents up to 200 A g^{-1} can be explained by the nanostructure and sheet dimensions of the synthesised $Na_{0.35}MnO_2$ that allow ion transport throughout the material that is not limited by solid state diffusion, in contrast to crystalline $Na_{0.35}MnO_2$ nanowires, where capacitance is shown to decrease significantly with the scan rate of CV.[15]

Conclusions

In summary, we present powders of 2D-ordered manganese dioxide that comprised of randomly distributed manganese oxide layers, size 2 × 4 nm, and sodium atoms located amongst them, also without forming a regular pattern. The dimensionality of the ordered domain is established by Debye refinement, an unrivalled tool for the task.

Due to such arrangement of the oxide layers, this ionic conductor was found to be genuinely pseudocapacitive, with charge storage not limited by diffusion of ions between stacked layers. Under substantial current rates, up to 200 A g^{-1}, a capacitance greater than 190 F g^{-1} was maintained. The material was incredibly stable, with no significant capacitance loss (<5%) after 5000 charge–discharge cycles.

The synthesised $Na_{0.35}MnO_2$ exhibits fast ion mobility due to the formation of short interlayers (2 × 4 nm) and significantly capacitance was found to be not limited by the solid-state diffusion. The distinctive material property is its capacitance retention at exceptionally high current rates, thereby opening up a new approach of material design to take full advantage of surface redox sites to store and deliver charge.

Acknowledgements

We would like to acknowledge the support of the European Commission FP7 Project "Stable Interfaces for Rechargeable Batteries" (SIRBATT) (FP7-ENERGY-2013, grant agreement No. 608502), the Royal Society and the Engineering and Physical Sciences Research Council (EPSRC) for the part funding of this research under Grant Numbers EP/K016954/1 and EP/N032888/1. The Ministry of Science and Technology, Taiwan (MOST 103-2911-I-007-515, 104-3113-E-006-005, NSC 102-2221-E-007-120-MY3) and the boost program from LCERC of National Tsing Hua University (NTHU) is acknowledged. We thank Diamond Light Source, UK for access to beamline B18 that contributed to the results presented here under BAG Proposal SP12120, PI Prof. Alan Chadwick and beam line scientist Dr Giannantonio Cibin. The Nanoinvestigation Centre at Liverpool (NiCaL) are acknowledged for access to the TEM. Part of the work was carried out within the cooperative framework set-up between NTHU, Taiwan and University of Liverpool, UK.

Notes and references

1 H. Y. Lee and J. B. Goodenough, *J. Solid State Chem.*, 1999, **144**, 220–223.
2 B. Babakhani and D. G. Ivey, *J. Power Sources*, 2010, **195**, 2110–2117.
3 Q. Qu, P. Zhang, B. Wang, Y. Chen, S. Tian, Y. Wu and R. Holze, *J. Phys. Chem. C*, 2009, **113**, 14020–14027.
4 T. H. Wu, Y. H. Chu, C. C. Hu and L. J. Hardwick, *Electrochem. Commun.*, 2013, **27**, 81–84.
5 J. Jiang and A. Kucernak, *Electrochim. Acta*, 2002, **47**, 2381–2386.
6 W. Wei, X. Cui, W. Chen and D. G. Ivey, *Chem. Soc. Rev.*, 2011, **40**, 1697–1721.
7 M. Toupin, T. Brousse and D. Bélanger, *Chem. Mater.*, 2002, **14**, 3946–3952.
8 S. Devaraj and N. Munichandraiah, *J. Phys. Chem. C*, 2008, **112**, 4406–4417.
9 C.-C. Hu, C.-Y. Hung, K.-H. Chang and Y.-L. Yang, *J. Power Sources*, 2011, **196**, 847–850.
10 T.-H. Wu, D. Hesp, V. Dhanak, C. Collins, F. Braga, L. J. Hardwick and C.-C. Hu, *J. Mater. Chem. A*, 2015, **3**, 12786–12795.
11 Q. Qu, L. Li, S. Tian, W. Guo, Y. Wu and R. Holze, *J. Power Sources*, 2010, **195**, 2789–2794.
12 S. He and W. Chen, *J. Power Sources*, 2014, **262**, 391–400.
13 J.-W. Wang, Y. Chen and B.-Z. Chen, *J. Alloys Compd.*, 2016, **688**, 184–197.
14 M. Huang, Y. Zhang, F. Li, L. Zhang, R. S. Ruoff, Z. Wen and Q. Liu, *Sci. Rep.*, 2014, **4**, 3878.
15 B. H. Zhang, Y. Liu, Z. Chang, Y. Q. Yang, Z. B. Wen, Y. P. Wu and R. Holze, *J. Power Sources*, 2014, **253**, 98–103.
16 H. W. Kroto, J. R. Heath, S. C. O'Brien, R. F. Curl and R. E. Smalley, *Nature*, 1985, **318**, 162–163.
17 S. Iijima, *Nature*, 1991, **354**, 56–58.

18 K. S. Novoselov, A. K. Geim, S. V. Morozov, D. Jiang, Y. Zhang, S. V. Dubonos, I. V. Grigorieva and A. A. Firsov, *Science*, 2004, **306**, 666–669.
19 L. Peng, Y. Zhu, D. Chen, R. S. Ruoff and G. Yu, *Adv. Energy Mater.*, 2016, **6**, 1600025.
20 P. Wei, S. Lee, F. Lemaitre, L. Pinel, D. Cutaia, W. Cha, F. Katmis, Y. Zhu, D. Heiman, J. Hone, J. S. Moodera and C.-T. Chen, *Nat. Mater.*, 2016, **12**, 554–561.
21 G. Fiori, F. Bonaccorso, G. Iannaccone, T. Palacios, D. Neumaier, A. Seabaugh, S. K. Banerjee and L. Colombo, *Nat. Nanotechnol.*, 2014, **9**, 768–779.
22 F. Bonaccorso, L. Colombo, G. Yu, M. Stoller, V. Tozzini, A. C. Ferrari, R. S. Ruoff and V. Pellegrini, *Science*, 2015, **347**, 1246501.
23 V. Nicolosi, M. Chhowalla, M. G. Kanatzidis, M. S. Strano and J. N. Coleman, *Science*, 2013, **340**, 122619.
24 A. K. Geim and K. S. Novoselov, *Nat. Mater.*, 2007, **6**, 183–191.
25 W. Wu, L. Wang, Y. Li, F. Zhang, L. Lin, S. Niu, D. Chenet, X. Zhang, Y. Hao, T. F. Heinz, J. Hone and Z. L. Wang, *Nature*, 2014, **514**, 470–474.
26 E. Navarro-Moratalla and P. Jarillo-Herrero, *Nat. Phys.*, 2016, **12**, 112–113.
27 P. Joensen, R. F. Frindt and S. R. Morrison, *Mater. Res. Bull.*, 1986, **21**, 457–461.
28 K. R. Paton, E. Varrla, C. Backes, R. J. Smith, U. Khan, A. O'Neill, C. Boland, M. Lotya, O. M. Istrate, P. King, T. Higgins, S. Barwich, P. May, P. Puczkarski, I. Ahmed, M. Moebius, H. Pettersson, E. Long, J. Coelho, S. E. O'Brien, E. K. McGuire, B. M. Sanchez, G. S. Duesberg, N. McEvoy, T. J. Pennycook, C. Downing, A. Crossley, V. Nicolosi and J. N. Coleman, *Nat. Mater.*, 2014, **13**, 624–630.
29 J. N. Coleman, M. Lotya, A. O'Neill, S. D. Bergin, P. J. King, U. Khan, K. Young, A. Gaucher, S. De, R. J. Smith, I. V. Shvets, S. K. Arora, G. Stanton, H.-Y. Kim, K. Lee, G. T. Kim, G. S. Duesberg, T. Hallam, J. J. Boland, J. J. Wang, J. F. Donegan, J. C. Grunlan, G. Moriarty, A. Shmeliov, R. J. Nicholls, J. M. Perkins, E. M. Grieveson, K. Theuwissen, D. W. McComb, P. D. Nellist and V. Nicolosi, *Science*, 2011, **331**, 568–571.
30 Y. Hernandez, V. Nicolosi, M. Lotya, F. M. Blighe, Z. Sun, S. De, I. T. McGovern, B. Holland, M. Byrne, Y. K. Gun'Ko, J. J. Boland, P. Niraj, G. Duesberg, S. Krishnamurthy, R. Goodhue, J. Hutchison, V. Scardaci, A. C. Ferrari and J. N. Coleman, *Nat. Nanotechnol.*, 2008, **3**, 563–568.
31 C. Sole, N. E. Drewett, F. Liu, A. M. Abdelkader, I. A. Kinloch and L. J. Hardwick, *J. Electroanal. Chem.*, 2015, **753**, 35–41.
32 X. Xiao, H. Song, S. Lin, Y. Zhou, X. Zhan, Z. Hu, Q. Zhang, J. Sun, B. Yang, T. Li, L. Jiao, J. Zhou, J. Tang and Y. Gogotsi, *Nat. Commun.*, 2016, **7**, 11296.
33 Z. Sun, T. Liao, Y. Dou, S. M. Hwang, M.-S. Park, L. Jiang, J. H. Kim and S. X. Dou, *Nat. Commun.*, 2014, **5**, 3813.
34 Z. Su, C. Yang, B. Xie, Z. Lin, Z. Zhang, J. Liu, B. Li, F. Kang and C. P. Wong, *Energy Environ. Sci.*, 2014, **7**, 2652–2659.
35 Y. G. Andreev and P. G. Bruce, in *Epdic 7: European Powder Diffraction, Pts 1 and 2*, ed. R. Delhez and E. J. Mittemeijer, Trans Tech Publications Ltd, Zurich-Uetikon, 2001, vol. 378-3, pp. 148–153.
36 P. Debye, *Ann. Phys.*, 1915, **351**, 809–823.
37 Y. G. Andreev, P. M. Panchmatia, Z. Liu, S. C. Parker, M. S. Islam and P. G. Bruce, *J. Am. Chem. Soc.*, 2014, **136**, 6306–6312.
38 Y. G. Andreev and P. G. Bruce, *J. Appl. Crystallogr.*, 2016, **49**, 24–30.
39 C. R. Fleeger, P. J. Heaney and J. E. Post, *Am. Mineral.*, 2013, **98**, 671–679.
40 T. Gao, H. Fjellvåg and P. Norby, *Anal. Chim. Acta*, 2009, **648**, 235–239.
41 C. M. Julien, M. Massot and C. Poinsignon, *Spectrochim. Acta, Part A*, 2004, **60**, 689–700.
42 K. W. Nam and K. B. Kim, *J. Electrochem. Soc.*, 2006, **153**, A81.
43 C. Julien, M. Massot, R. Baddour Hadjean, S. Franger, S. Bach and J. P. Pereira-Ramos, *Solid State Ionics*, 2003, **159**, 345–356.
44 A. Dias, R. G. Sá, M. C. Spitale, M. Athayde and V. S. T. Ciminelli, *Mater. Res. Bull.*, 2008, **43**, 1528–1538.
45 D. Chen, D. Ding, X. Li, G. H. Waller, X. Xiong, M. A. El-Sayed and M. Liu, *Chem. Mater.*, 2015, **27**, 6608–6619.
46 Y. K. Hsu, Y. C. Chen, Y. G. Lin, L. C. Chen and K. H. Chen, *Chem. Commun.*, 2011, **47**, 1252–1254.
47 Q. T. Qu, Y. Shi, S. Tian, Y. H. Chen, Y. P. Wu and R. Holze, *J. Power Sources*, 2009, **194**, 1222–1225.
48 L. Mai, H. Li, Y. Zhao, L. Xu, X. Xu, Y. Luo, Z. Zhang, W. Ke, C. Niu and Q. Zhang, *Sci. Rep.*, 2013, **3**, 1718.
49 K. W. Kim, M. G. Kim and K. B. Kim, *J. Phys. Chem. C*, 2007, **111**, 749–758.